Journal of Inorganic and Organometallic Polymers and Materials (2023) 33:2835–2847
https://doi.org/10.1007/s10904-023-02715-8

RESEARCH

The Role of Polyethylene Glycol, a Water Entrainer on Characteristics of Silico Alumino Phosphate Geopolymer to Harvest Enhanced Gel Phase and Stability

N. Vanitha[1] · R. Jeyalakshmi[1]

Received: 5 April 2023 / Accepted: 13 May 2023 / Published online: 1 June 2023

Abstract
Geopolymers display a typical brittle mechanical behaviour with low ductility and low fracture toughness. These properties might represent a significant limitation for structural applicationsoffers steric entrapping of the organic molecule and thus structuring the solvated cations in the solution so as to enhance the hydrogen bonding between organic polymer and oxides in the inorganic framework. Research efforts have been done on the use of soluble organic polymer in alkali-activated geopolymers in general but studies on their role in phosphate elaborated geopolymers are rare. In view of the above, this research investigates the preparation of the Polyethylene glycol /Metakaolin geopolymer with silico alumino phosphate gel structure under ambient curing conditions and its performance compared with control samples cured at ambient as well at 80 °C temperature. The effect of PEG at different doses 0–3% (MKGP1, MKGP2 and MKGP3) in metakaolin reaction under phosphoric acid of molarity 10 M was studied by measuring compressive strength, flexural strength while tracing and identification of the formed gel network by employing X-ray diffraction, FTIR and Scanning electron microscopic analysis. Strength analysis showed an enhancement with about more than 50% gain in compressive strength in polymer-assisted samples than that of the control samples (MKGP0) which were 12.1 MPa at (ambient) 18.8 MPa at 80 °C curing. XRD assemblages and FTIR spectral data proved an increased amorphous gel with PEG addition of up to 3% with the refinement of pores. Dense microstructure in blended samples was evident from SEM analysis. The total weight loss by heating the samples in TGA / DTA was found to be lower in PEG samples (29%) and for control mixes as high as 49%. The study results offer valuable organic-geopolymeric composites with better mechanical properties that can be applied for various potential applications as coatings, restoration and conservation domain.

✉ R. Jeyalakshmi
jeyalakr@srmist.edu.in; rajyashree64@gmail.com

N. Vanitha
Vn5425@srmist.edu.in

[1] Department of Chemistry, College of engineering and technology, SRM Institute of Science and Technology, Kattankulathur, Tamil Nadu 603203, India

Graphical Abstract

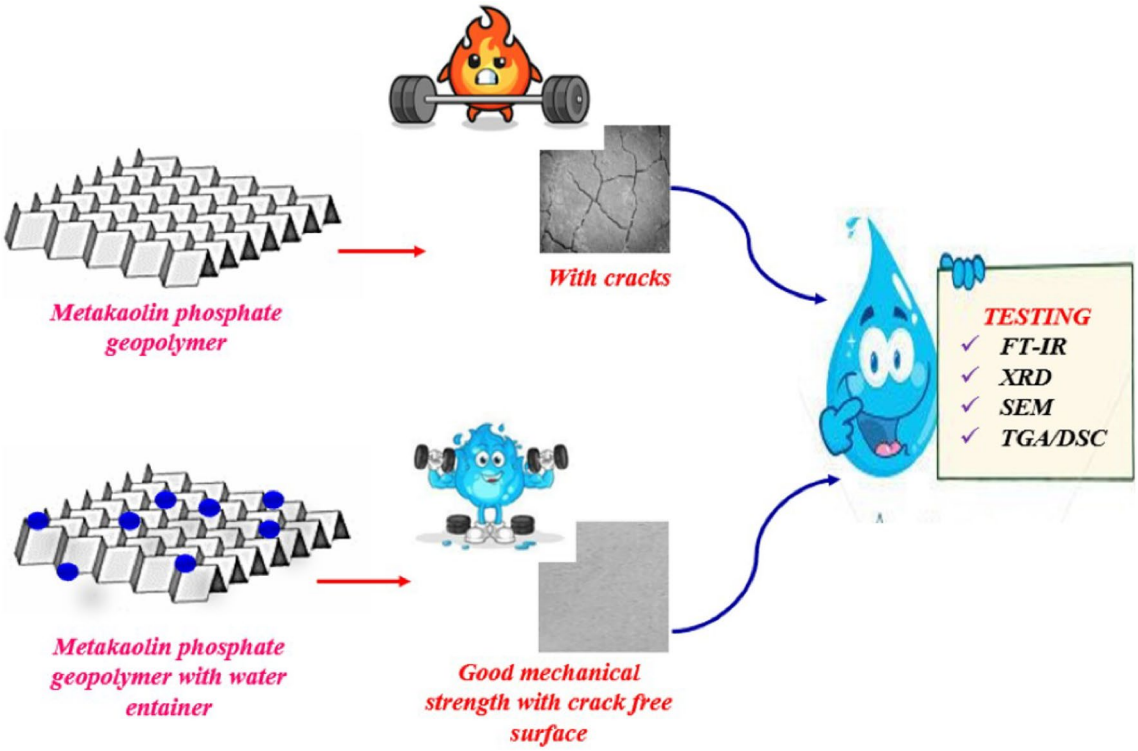

Keywords Phospo geopolymer · Metakaolin · Polyethylene glycol · TGA · DSC · XRD

1 Introduction

Geopolymers, an inorganic material used as an alternative binder for ordinary Portland cement, are prepared from widely and abundantly available clay minerals, and industrial by-products containing alumino silicate materials [1–3]. Owing to their mechanical, and chemical characteristics and three-dimensional structure [4, 5], the geopolymers are capable of binding aggregates, removing and immobilizing heavy metals, ceramic-type materials, etc. They are also stable in a wide range of pH, thermally treated at elevated temperature exposure as well as resistance to water and aggressive chemicals [6, 7]. The characteristics and properties mainly depend upon the nature of the network present in turn nature of the chemical bond in raw materials and activating agents. Generally, geopolymers are a two-component system, comprising solid aluminosilicate precursor and activation solution either alkaline or acid medium [8]. The far most used activators are alkali silicate, hydroxide, and water or phosphoric acid solutions in different concentrations. Homogenization of optimized material yield geopolymer cement with properties similar to Portland cement paste or even superior in particular cases viz., thermal stability, encapsulation of heavy metals, resistance to aggressive chemicals and corrosion resistance, etc. [9, 10].

The mechanism of geopolymerization is described in the following overlapping stages: dissolution of the precursor; equilibrium, gelation, reorganization, polymerization, and hardening [11–13] (Fig. 1).

All these reactions are occurring concurrently and in this way, they exhibit a wide variety of properties, such as high mechanical strength [14], low shrinkage, fast or slow setting, acid, and fire resistance [15], low thermal conductivity, long term durability, and thermal stability [16]. To these characteristics, geopolymers have a wide range of potential applications in diversified fields such as thermal stability, dielectric, cathode battery material, and water resistance. Despite their unique properties and potential as geopolymers, the materials have yet to get into the market and gain general acceptance in mainstream applications. It is mainly from the different types of source materials from industrial wastes or natural/activated clay types that widely vary in their chemical composition, mineralogy, and properties. Much of the work reported on the effect of the chemical composition of the raw materials and hardeners for structural applications. The basic

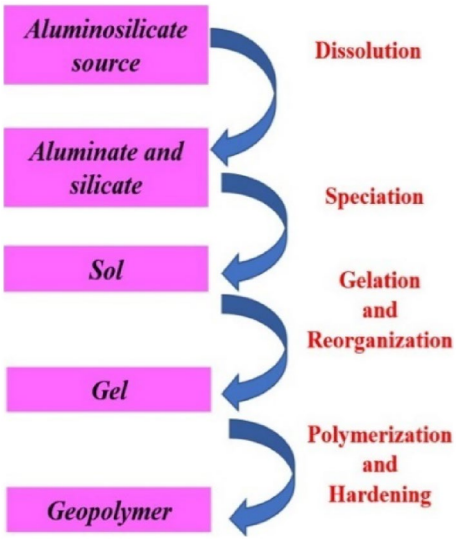

Fig. 1 Schematic representation of various stages involved in the geopolymerisation reaction

need for functional properties is mechanical strength, low shrinkage, and high durability against thermal and aggressive chemicals. To achieve these desirable properties, the base matrix should be dense, crack-free bulk structure, and easy fabricability [17].

To the reports available in phosphate-based geopolymer technology, known to be silico alumino phosphate (SAP) are more attractive and presented new properties than traditional alkali-activated geopolymers such as thermal properties, shrinkage, and water resistance [18–20]. For this type, raw material mainly metakaolin, a calcined kaolinite clay, is attacked by orthophosphoric acid and hardened by hot curing or ambient curing. The phosphoric acid solution comprises H^+ protons and H_2PO^{4-} ions in which H^+ ions protonate oxygen thereby breaking the Al–O–Al network at the beginning of the reaction step followed by polycondensation reaction. Studies on the structural network and the effect of acid content on the metakaolin show the formation of $AlPO_4$ and $[Al_2(PO_4)(OH)_3]$ phases at room temperature [21, 22]. At a molar ratio, Al/P is unity, alumino phosphates, and ortho alumino phosphates $Al(PO_4)^3$ along with a hydrated form of $Al(H_2PO_4)^3$ phase reported in the early work. As most of the works reported on the hardening of metakaolin under an acid medium at a high energy gradient process. The optimized strength in the range of M30–M40 was attained under hot curing conditions, less than 80 °C temperature at 28 days. Under hot curing the prepared geopolymer undergoes some physical changes that end up with more micro and macro cracks in the bulk [23, 24]. Hence matrix lost its visual appearance followed by spalling or peeling of the surface. Even, self-desiccation which may cause by improper curing seriously affects the strength and durability of the concrete. This could be avoided by the addition of some curing agents to slow down the self-curing process [25].

Some of the inorganic additives like alumino silicate materials or phosphates help to produce specimens at room temperature but they resulted in a reduction of the compressive strength [26, 27]. Few organic chemical additives to increase the elasticity and toughness are recommended and known for their improved self-curing properties. They are mostly water-soluble polymers like polyvalent alcohol, selected from the group consisting of polyethylene glycol (PEG), Propylene glycol (PG), DI-propylene glycol (DPG), Butylene glycol, Neopentyl glycol (NPG), Xylitol, Sorbitol, and Glycerine; or Phytosterols, Polyoxymethylene (POE), Sodium Pyrrolidone Carboxylate (PCA-Na), Hyaluronic acid, Stearyl alcohol, Acetyl alcohol or Polyacrylic acid are recommended [28]. By comparing with conventional curing, the self-curing agents reduce water evaporation from concrete, increase the retention capacity of moisture and prevent early-age cracking [29–31].

In view of the above, this study aims to solve the ill effects due to self-desiccation and reduce the thermal gradient in the processing of acid-elaborated geopolymer by the inclusion of an organic polymeric phase to develop shrinkage-free hybrid geopolymer. Towards that, Polyethylene glycol, a polyether compound, commonly expressed as $H–(O–CH_2–CH_2)_nOH$ selected as an additive. Most studies on ordinary Portland cement with PEG as a self-curing agent focus on strength development and durability changes while ignoring the thermal property changes brought about by PEG itself. Though PEG is known as a phase change material, having a phase transition temperature of 20–35 °C with a wide range of enthalpies (91.72–105.70 J/g) utilized in ordinary Portland cement. The PEG—metakaolin biphasic composites from alkali activation has been reported [32]. The interaction between these two is characterized by weak hydrogen bonds through the interpenetration of organic polymer into the inorganic polymer at the micro-scale level. These bibasic composites modify the mechanical properties by influencing the reaction's evolution and thus more Si–O–Al bonds in the alumino silicate framework. But the maturation of the matrix is attained at a minimum of 28 days.

Since the mechanism of the alkali mediation and acid elaboration of the metakaolin are completely different, hence there is a need for thorough investigation. During the alkali attack, the dissolution of Silica and alumina from metakaolin simultaneously involved in the concurrent oligomerization and polycondensation. But in the case of an acid attack, the dissolution of alumina from metakaolin is faster compared to Si and thus fast formation of Al–P gel covering metakaolin particles at elevated temperature of curing during the first stage of the reaction. The heat evolved during this period is high and the risk of thermal cracking is more. Therefore, this

study aims to obtain SAP samples with high reaction degrees at ambient temperature by avoiding cracking and shrinkage with the aid self-curing agent, PEG was proposed. Due to the absence of any report on its utilization in geopolymers, there is a need to highlight this material and its capabilities in a new binder. When the PEG a soft segment incorporated into inorganic hard cement, it adds chemical stability, fire resistance, and thermal conductivity due to the change in the bulk as well microstructure. Hence the role of this additive on the degree of the reaction assessed in the optimum dose of the PEG under ambient curing conditions. The functional groups and morphologies were monitored using infrared spectroscopy and scanning electron microscopy respectively.

2 Materials and Methods

Metakaolin, alumino silicate obtained from thermally activated kaolinite clay used in this study as a solid source material for geopolymerisation. The chemical composition of metakaolin was found to be 90% of Si and Al oxide. To elaborate on the solid source, hardener, Orthophosphoric acid (AR grade 85%) of 10 M solution was utilized. Water soluble polymer, Polyethylene glycol, PEG 400 was sourced from Southern India Scientific Corporation as a water entrainer. Geopolymers paste samples were prepared as two series with and without the addition of Polyethylene glycol. The control mixes were first cured under a slightly elevated temperature at 80 °C ($MKGP^{80}$) as well ambient temperature, MKGP0. The paste slurry was prepared in digi mortar by mixing solids thoroughly for 5 mins followed by the addition of 10M prepared orthophosphoric acid and then homogenized mechanically for 10 mins. PEG 400 was added at the dosage of 1, 2, 3% (MKGP0 -MKGP3) in the second series by mixing them mechanically in the phosphoric acid and cast in the 50 mm cube size mould, cured at ambient conditions only. All the tests were conducted after curing at 14, and 28 days of air annealed samples.

3 Characterization Studies

The XRD pattern was collected using a Phillips diffractometer, model X-pert using Cu-Kα radiation by scanning from 10° to 80° (2θ) at a scanning speed of 2°/min and at a step size of 0.02°. The crystallographic phases were identified with JCPDS cards and also with High Score Plus software. FT-IR spectra were recorded using Bruker IFS 66v/S FT-IR spectrometer with KRS-5 lens and ATR accessories. The transmittance spectra were recorded in the range of 4000–400 cm^{-1} at a resolution of 2 cm^{-1} and a scanning speed of 5 kHz with 32 scans. Field emission scanning electron microscopy (FESEM) using JEOL JSM 6300 microscope with a tungsten filament electron source and 20 kV accelerating voltage. An X-ray spectrometer [energy dispersive spectroscopy (EDS)] was employed to determine the chemical compositions of the phases identified. Atomic Force Microscopic studies were used to determine surface morphology by park systems corporation XE7 in contact mode. Thermogravimetric analysis and Differential scanning calorimetry (TGA and DSC) studies were conducted for a simultaneous thermal analysis (STA) in NETSCH 2500 Regulus in the temperature range of 30–1000 °C in floating air/nitrogen (60 ml/min) at a heating rate of 10 °C/min. The compressive strength of the paste and mortar specimens was determined using a digital compressive machine following the ASTM C39-20 standard and flexural strength following measured according to ASTM C78-18.

4 Results and Discussion

The development of compressive strength, the flexural strength of the metakaolin phosphate-based geopolymer (MKGP) and of the PEG–MK geopolymer (MKGP1-MKGP3) are presented in Figs. 2 and 3. The strength enhancement of MKGP attained from 20.7 to 46.2 MPa while subjecting the samples to hot curing $MKGP^{80,}$ Further, the addition of PEG improved the strength of ambient cured samples at both ages and found to be maximum at 2% of PEG 400. Further addition of PEG did not help much to the strength development. A similar trend is observed in the flexural strength of geopolymer samples. The mechanical improvement resulting from the incorporation of the PEG was remarkable and compressive strength was increased by 37.1 MPa (MKGP2) which was 50 times greater than MKGP0 (20.1 MPa). It can be argued that the interfacial adhesion between geopolymer and the organic polymer

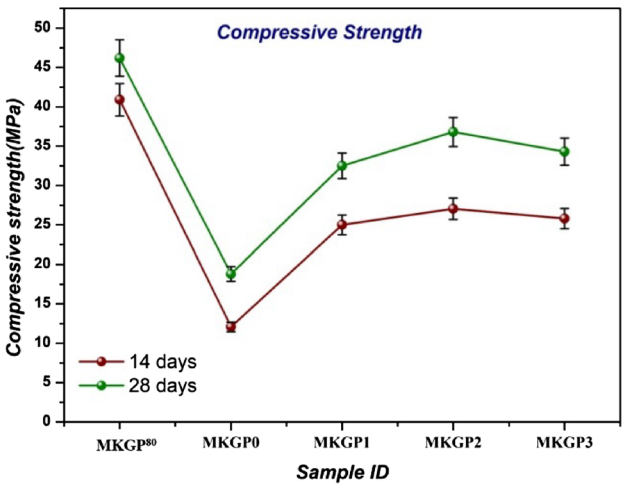

Fig. 2 Compressive strength of geopolymer

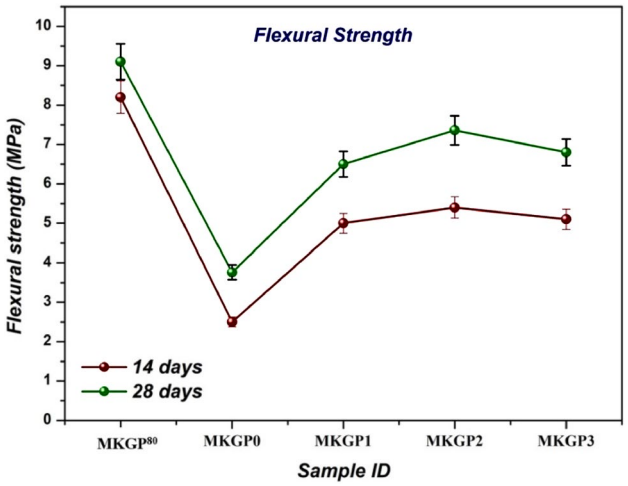

Fig. 3 Flexural strength of geopolymer

is more as well the weak interaction between the weakly polar character of PEG due to the presence of OH group and methylene groups, compared with the hydrophilic and polar surface of GP due to presence of …H–Si–O–Al–O–P– type bond. It can be further elaborated from AFM and SEM analysis.

The effect of organic polymer addition on the changes in the XRD pattern verified and the diffractograms are, presented in Fig. 4.

X-ray diffraction pattern of metakaolin (MK) conforming the peaks of crystalline phases that correspond to Quartz and Anatase along with a broad hump of amorphous phases in the range 17° and 32° (2θ) centered at around 25° (2θ). The characteristic reflection of Quartz 20, 25, 26, 40° (2θ) and Anatase (36°), identified from PDF (74-1811) and PDF (21-1272). The XRD pattern of $MKGP^{80}$ sample illustrates the broadening of the amorphous region between 18 and 34° 2θ values with the slight displacement of these 2θ values toward a higher degree 2θ compared to raw material. The typical halo hump extended from 17° to 39° 2θ while the MK-PEG geopolymers conformed a higher degree of amorphous silico alumino phosphate (SAP) network that coincided with enhanced mechanical strength.

From this, it is clear that organic PEG polymer increasing the incorporation of phosphate ions into the alumino silicate network by slow curing, entails the formation of poly(phospho-siloxo) –Si–O–P–O–Si– 3D network materials generally reported in phosphate geopolymers [27, 33].

The X-ray pattern of PEG blend geopolymer cement with reference to ambient cured control samples is presented in Fig. 5. It shows the newly formed crystalline phase of berlinite or aluminium phosphate ($AlPO_4$) main and sub-peaks that formed from leaching Al in acid followed by its reaction with phosphate units. Berlinite is isostructural with quartz and some peaks of this new crystalline phase are superimposed with the ones of quartz. The polymorphs of $AlPO_4$, (berlinite) type is seen at 2θ values of 20°, 25°, 27°, 29°, 31° and 39° corresponding to aluminum phosphate (PDF 10–423) and some hydrated form of aluminum phosphate reflections at 49° 2θ value [$Al(H_3PO_4)_2.3H_2O$) (PDF 00-020-0010)] are identified in all the specimens [23, 24, 34]. The nature of the chemical bonding present is further assessed from FTIR studies.

5 Functional Group Studies

The infrared spectrum of MK in Fig. 6 shows a sharp band at 1051 cm^{-1} which is from a tetrahedral unit of Si–O–T (T = Si or Al) vibration and the peak at 800 cm^{-1} is from Al–O–T (T = Si or Al) vibration. Peaks at 518 and 413 cm^{-1} are attributed to the stretching vibration of Si–O and amorphous silica. Hot cured sample ($MKGP^{80}$) shows a sharp increase in the wavenumber of Si–O–T at 1062 cm^{-1}, a positive shift from that of MK but this shifting of the band

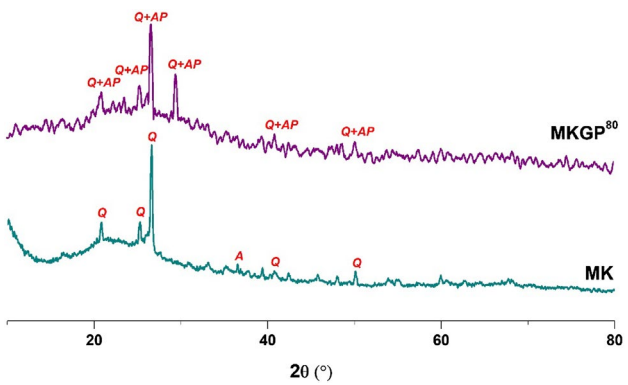

Fig. 4 XRD of Metakaolin and $MKGP^{80}$

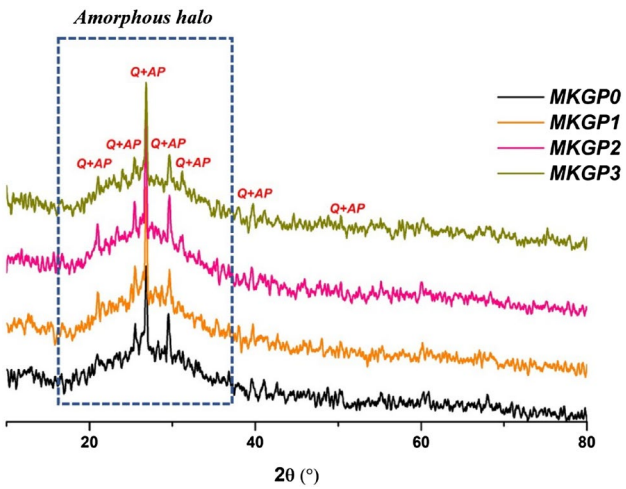

Fig. 5 XRD of Phosphate geopolymer and PEG-assisted geopolymer

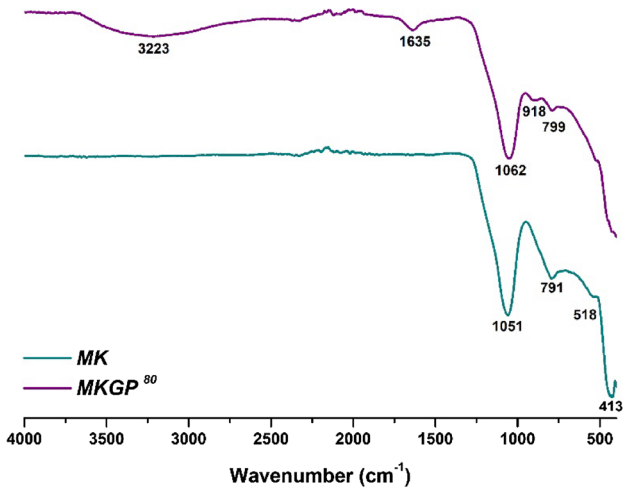

Fig. 6 FT-IR of Metakaolin and MKGP^{80}

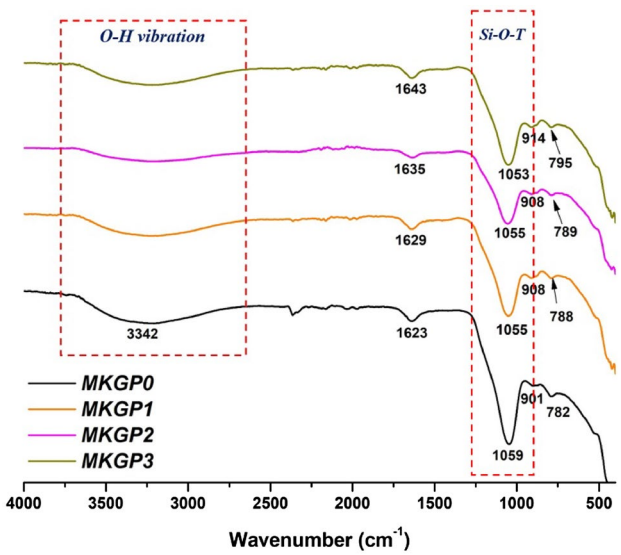

Fig. 7 FT-IR of phosphate geopolymer

is not very effective in ambient cured samples.; MKGP0 at 1059 cm^{-1}. In the case of polymer added sample series, (MKGP1-MKGP3), Si–O–T bonds frequency settled at 1059 cm^{-1} to 1053 cm^{-1}, suggesting that the product formed are richer in Al–O–Si than Si–O–Si bonds compared to PEG-free geopolymer sample. A broad O–H band from 3100 to 3668 cm^{-1} in all geopolymer samples shows Si–OH and P–OH absorption. Other peaks at 900–915 cm^{-1} correspond to P–O vibration bands associated with the Al–O–P network. Almost all samples show P–O, Si–OH, and O–H vibration around 1600 cm^{-1}. The formation of the poly(phosphosiloxo) chain in the system is confirmed by the newly formed band at 780–795 cm^{-1} in all geopolymer samples which is attributed to Si–O–P as suggested by literature reports [23, 27, 35] (Fig. 7).

6 Thermal Studies

Thermal analysis (TGA) was performed and the TG curves of geopolymer cement are represented in Fig. 8. Three types of water will escape during the heating such as physically bonded water, chemically bonded water, and hydroxyl groups. Water evaporation and dehydroxylation are probably the effects liable for the mass loss during heat treatment of geopolymer. In the TGA curve, at a low-temperature range, a broad endothermic peak was observed related to the loss of water molecules. Usually, physically bonded water evaporated at the temperature range between 25 and 100 °C, and this band is also known as the free water evaporation zone. Temperature between 80 and 100 °C, some of the water gets evaporated from the large pores present in the product. This endothermic phenomenon and the mass loss that appeared in all

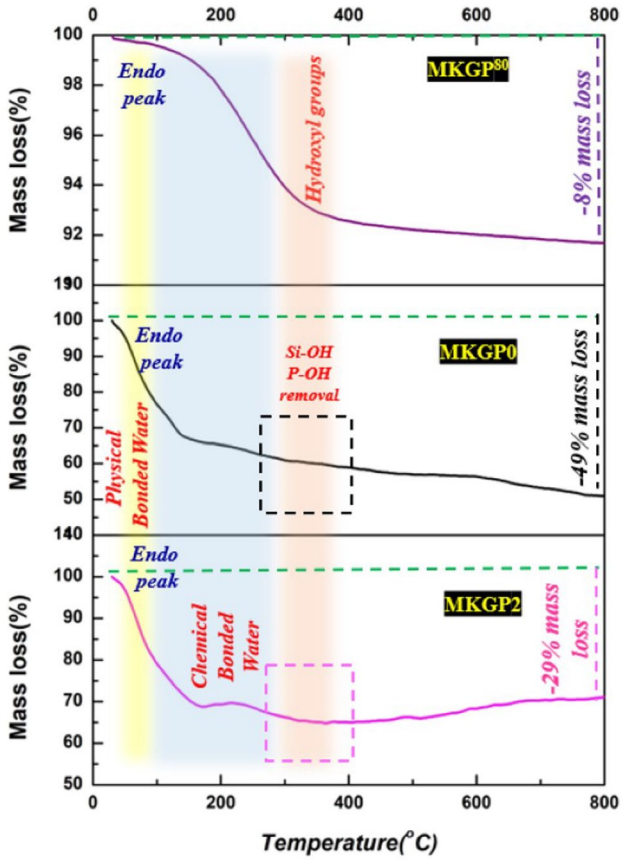

Fig. 8 TGA of metakaolin phosphate geopolymer

geopolymer cement indicate the removal of physically absorbed water, physically bonded water, and one part of the chemically bound water in the poly(phospho-siloxo) network. Chemically bonded water release was found at 169 °C in MKGP^{80}, 139 °C in MKGP0, and 165 °C in MKGP2. Consequently, the weight loss in the temperature range between 100 and 230 °C is from metastable phases which contain free water that can be linked to hydrated aluminophosphates. This might be from the P–OH groups formed from the reaction of hydroxyl groups released from H_3PO_4 with soluble alumino silicates from metakaolin [36].

Variation in the peak temperature in the TG curve of control samples cured at two different temperatures, say 316 °C in MKGP^{80}, and 307 °C in MKGP0 can be explained by the fact of bonding water molecules are higher in the ambient cured one. In a similar trend, PEG-assisted matured samples MKGP2 also showed a mass loss at a higher temperature, 320 °C. At the same time the peak characteristics for the dehydration of PEG normally observed around 494 °C have not been observed in our studied samples. This implies the added PEG utilized during the geopolymerisation. [24, 36]. Comparing the PEG loaded to that of control, a slight degree of mass loss was found at the temperature range between 250 and 300 C. This might be from dehydration of Si–OH which was held by the hydrogen bond of PEG with the vicinal Si–OH molecule. Thermal reactions were further analyzed from DSC curves.

DSC analysis was carried out for samples from room temperature and presented in Fig. 9. A temperature lower than 300 °C, two endothermic peaks are clearly evident, one at 120–125 °C and another in the temperature range 140–150 °C in ambient cured samples of both control and MKGP2. On the other hand, hot cured control samples release the heat at 107 °C as a broad peak and another small peak at 40 °C. The differences between hot curing to that of room temperature are the content of water molecules in the geopolymeric network and/or physically bound one. Therefore, the occluded water molecule release at a slightly higher temperature over and above 110 °C in the MKGP2 and MKGP0 implied that these metakaolin phosphate geopolymer cements contain these aforementioned water molecules in their network even at relatively high temperatures. Therefore, these specimens could have a good high-temperature performance than hot-cured control samples. This is in good agreement with IR spectra results which show the absorption bands at about 1630 and 3600 cm^{-1} for –OH bonds as depicted in Fig. 7. At the same time, the hydroxyl group in Si–O–P–OH associated with incorporation of Phosphate ions, verified from the band at 799 cm^{-1} observed in the hot cured samples whereas, organic moiety associated HPO^{4-} ions accelerate the P–OH bond that in turn shift this

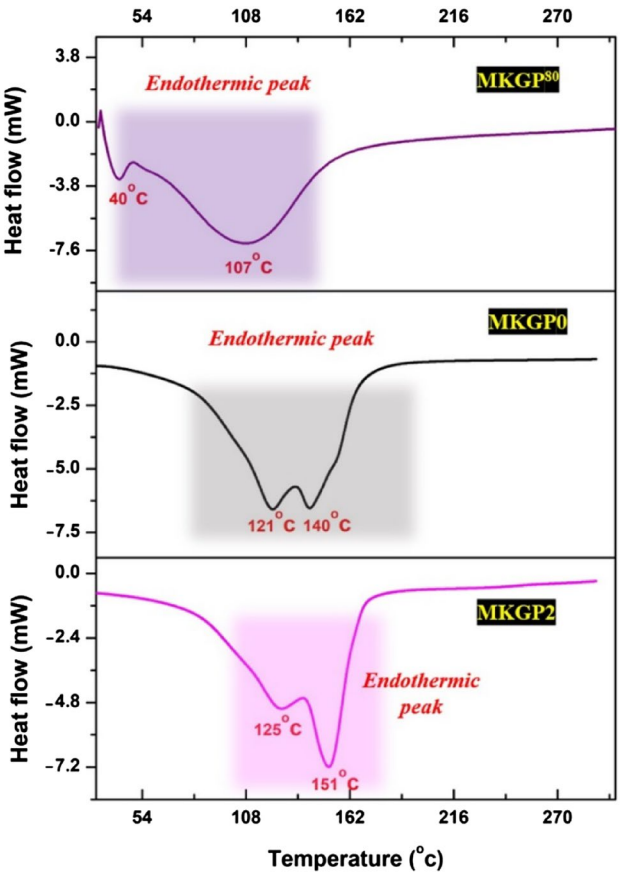

Fig. 9 DSC of metakaolin phosphate geopolymer

frequency number to a lower value (790 cm^{-1}) in PEG added samples [37, 38].

A common way of preparing phosphate-based MK-GP is an optimum of 70–80 °C temperature because the setting time of MK and H_3PO_4 solution is usually too long more than 48 h at room temperature. The hot curing process was found to be unfavorable, due to a larger amount of amorphous gel generated by Al^{3+} and PO_4^{3-} at a higher curing temperature, which hinders the further reaction and leads to a lower compressive strength. Similarly, a low degree of MK dissolution under acid reaction yields low Al content at room temperature or below 40 °C, hence did not yield strength at early ages, even in a few cases, it is nearly 8–10 MPa at the standard age of 28 days curing. Thus, it has been noticed that curing temperature is one of the critical parameters for the final compressive strength of the SAP samples.

It has been found in the literature [39] that the recommendation of a multi-stage curing process for SAP preparation to arrive the uniform strength. It is also believed that the cracking of the samples cured constantly at 60 and 80 °C is majorly attributed to the thermal expansive force induced by the great internal temperature rise of the samples. Though the higher curing temperature achieves strength and directly

increases the time of reaction, but the exothermic heat generated by vigorous reaction in a short time cannot be removed, leading to a great rise of the internal temperature and thus the expansive cracking of the matrix. In order to avoid such shrinkage, PEG, a water entrainer is used in this study and established the improvement in the strength. The mechanistic steps involved in the reaction has been shown in Fig. 10.

Tests were conducted by subjecting the MKGP0 and MKGP2 samples to the temperature of 100 °C for a sustained period of 2 h. The air-annealed samples were verified for their compressive strength. The MKGP0 completely lost their physical integrity and a few samples (2 out of 6) showed a marginal value of strength in the range of 7.5–8 MPa. On the other hand, no change in strength attainment was observed in PEG-assisted MKGP2 (35.6 MPa). From this, it is clear that the PEG-assisted ambient curing method of consolidation is effectively bonded silico alumino phosphate gel with retention of aluminium phosphate crystalline phases. Though XRD reflections of MKGP0 contain broad amorphous peaks that might be from both metakaolin as well their converted product of silico phosphates upon heating, the loss of water molecules destruct the gel structure [40].

The thermal degradation steps can be proposed from TG curves and DSC thermograms.

(i) The endothermic phenomenon and mass loss which appear between room temperature to 300 °C for all geopolymeric samples are from the removal of physically absorbed/bonded water with part of the chemically reacted molecule in the gels.

(ii) Comparing the mass loss of heated and unheated samples, lower degrees are observed in heated samples, or in other words, typically water molecules in the microstructure are less, and hence strength is more.

(iii) The unheated control samples as well as PEG-geopolymer composites, undergo heavy mass loss because of the abrupt loss of a higher amount of physically/chemically bound water, which could be responsible for lower strength.

(iv) Further mass loss above 600 °C is more in the case of unheated MKGP0 and MKGP2 could be assigned to the deterioration of P–OH groups in the structure of metakaolin phosphate gel. Comparing these two samples, the mass loss is heavy at unheated than at PEG-assisted. Thus, it is clear extended condensation reaction took place in the MKGP2 cement. This is also clarified by the observed peak corresponding to P-OH at 908–916 cm^{-1}.

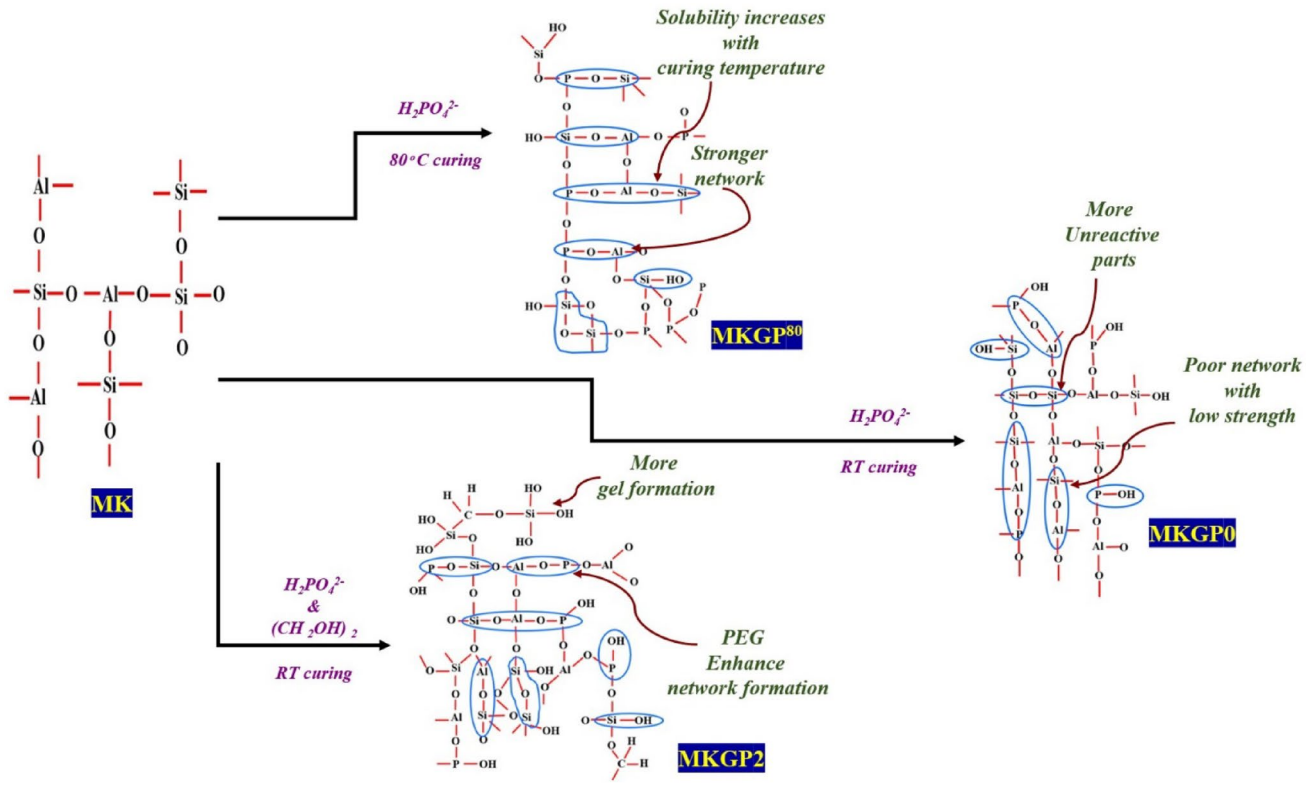

Fig. 10 Network formation in metakaolin phosphate geopolymer with and without PEG

Further micrograph assessment from SEM results has been carried out and analysed.

7 SEM Morphological Analysis

SEM micrograph of all matured geopolymers recorded after 28 days and presented along with elemental analysis in Fig. 11. It can be observed that most of the MK raw material reacted under acid attack, forming a dense gel with a compact structure in the heat-cured matured $MKGP^{80}$ samples. SEM picture of MKGP0 showed unreacted MK in lamellar structure. In PEG-added samples, high connectivity of gel with fewer pores is observed as it ascertaining the role of the organic phase in the geopolymerisation condensation reaction. It is understood that metakaolin can be reacted with phosphoric acid to convert most silica, aluminium, and calcium oxides into hydrogen phosphates, phosphates of the crystalline and or amorphous phase [24]. The presence of these was established from the XRD pattern and FTIR functional group analysis. The distribution of the phosphates in solid phases is affected by the interlacing of PEG at the ambient curing process which can be clearly distinguished from the SEM picture. The elemental mapping results indicated in Fig. 11 showed that all the geopolymers consist mainly of Si, Al, P, and O elements that were evenly distributed within the matrix. It indicates the formation of the Si–O–P–O–Al network [41]. EDS spectrum of specimens cured at elevated temperatures showed that Al/P and Si/P are much higher than ambient cured samples because the higher temperatures accelerate the dissolution and slowly transformed into diffusion controlled, even lowering the final reaction degree to some extent [42, 43].

The highly porous structure with more metakaolin particles indicates in MKGP0 the MK was not attended in the geopolymerisation while biphasic PEG composite, MKGP2, cured at ambient temperature exhibit much denser with a lower Al/P ratio and higher compressive strength. The average Al/P is approximately 1.0 ± 0.1 which is approximately equal to 1 probably indicating the formation of more $AlPO_4$ phase. This is further confirmed by the absence of PO_4 units from excess phosphoric acid normally appeared in the IR frequency range in the main band nearly at 1150 cm^{-1}. Therefore the balanced charges of PO_4^{3-} with Al or Si affect positively the network. This can be explained by following an interactive gel reaction from the added PEG. The depolymerisation of MK particles led to Al–OH units in the presence of an acid, entering into the reaction with the PO_4 tetrahedral unit. At the time of mixing, the PEG polymers are added to the slurry, mainly forming the hydrogen bonds between the water molecules, this helps to reduce the chemical potential of the molecule due to the reduction of the vapor pressure and the rate of evaporation from the exterior surface [44]. In other words, the moisture loss due to the continuous evaporation of the water due to the variation in the chemical potential and the free energy space between the liquid and the vapor phase is avoided by the incorporation of PEG.

SEM cannot completely reflect the fluctuation of the specimen surfaces, as the signals received are generally shown in grey diagrams, with no information about the surface variation. On the other hand, AFM is effective in the detection of nanometer spatial resolution and force sensing sensitivity, which can measure the surface morphology, as well as reflect the mechanical properties. Hence AFM images of the specimens of selected regions from SEM pictures to study topography. The AFM images are presented along with respected specimen SEM micrographs of the gel structure seen in geopolymer specimens analysed through AFM images are presented. The variation in the images is found in $MKGP^{80}$, MKGP0, and MKGP2. It is seen that the micro topology of the MKGP2 is smooth than samples without PEG. The visible deep cracks on the $MKGP^{80}$ sample in addition to the phase images are found with meso-structured

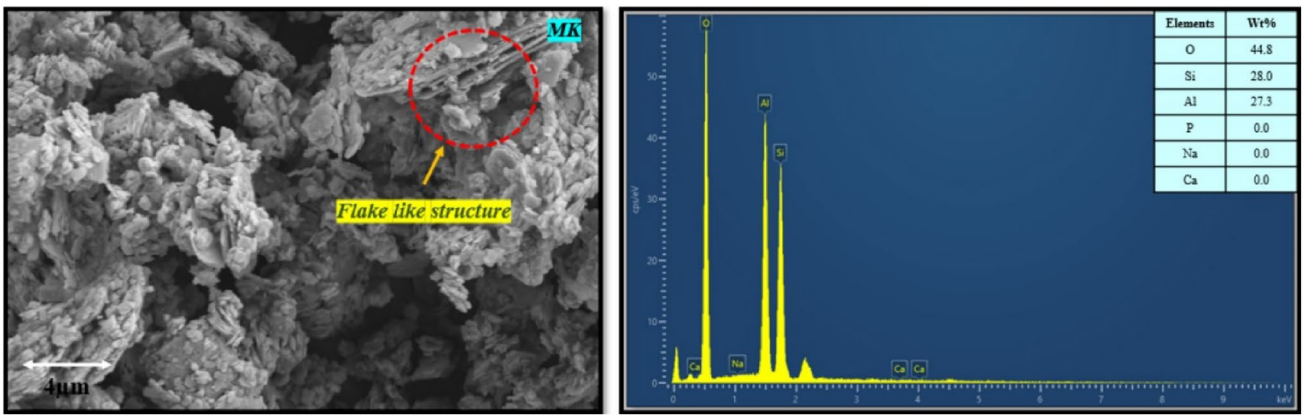

Fig. 11 SEM micrograph of MK

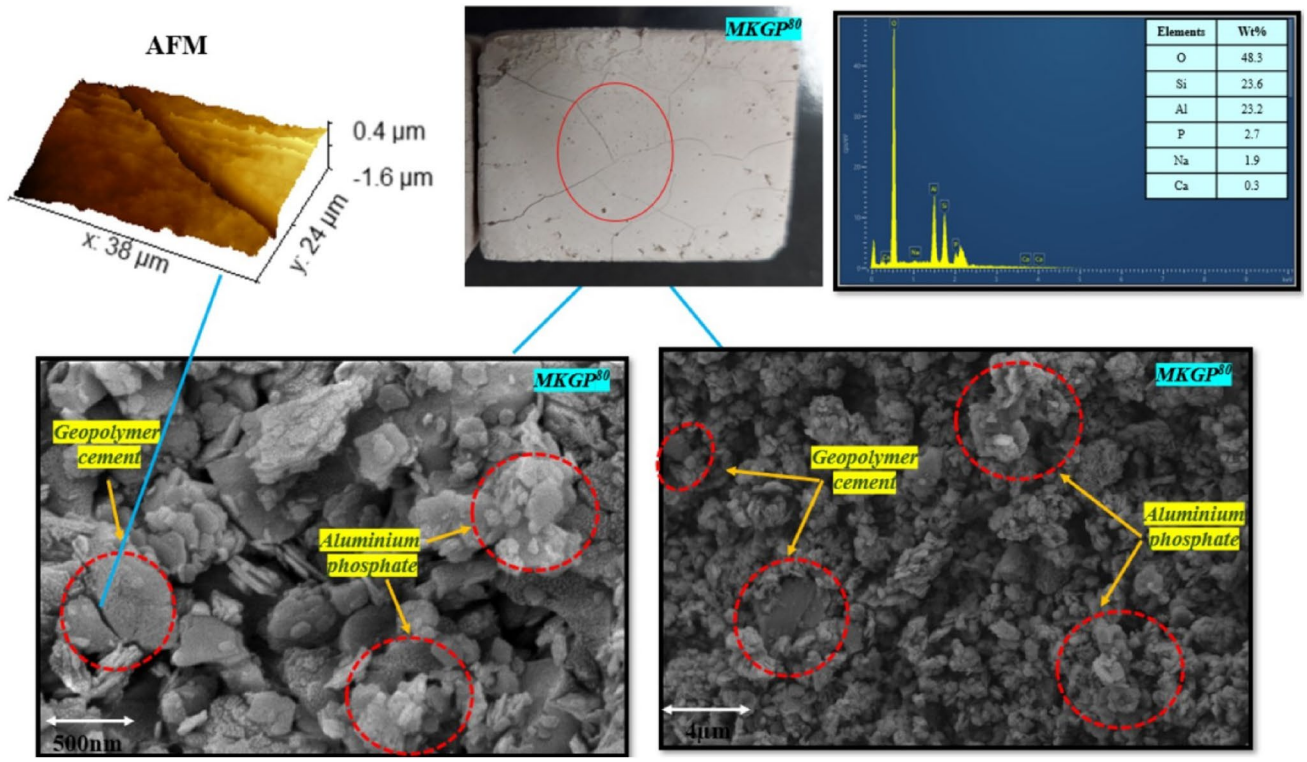

Fig. 12 AFM and SEM micrograph's of $MKGP^{80}$

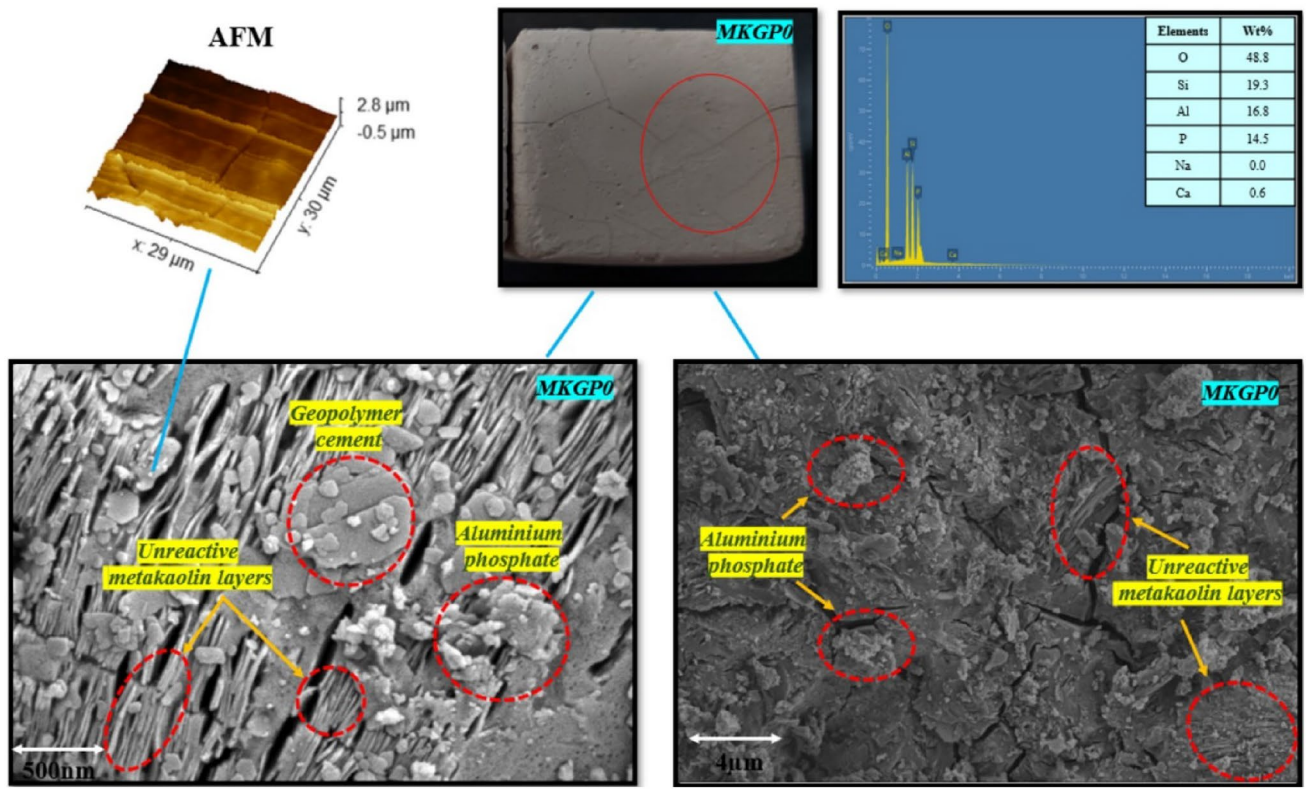

Fig. 13 SEM and AFM micrographs of MKGP0

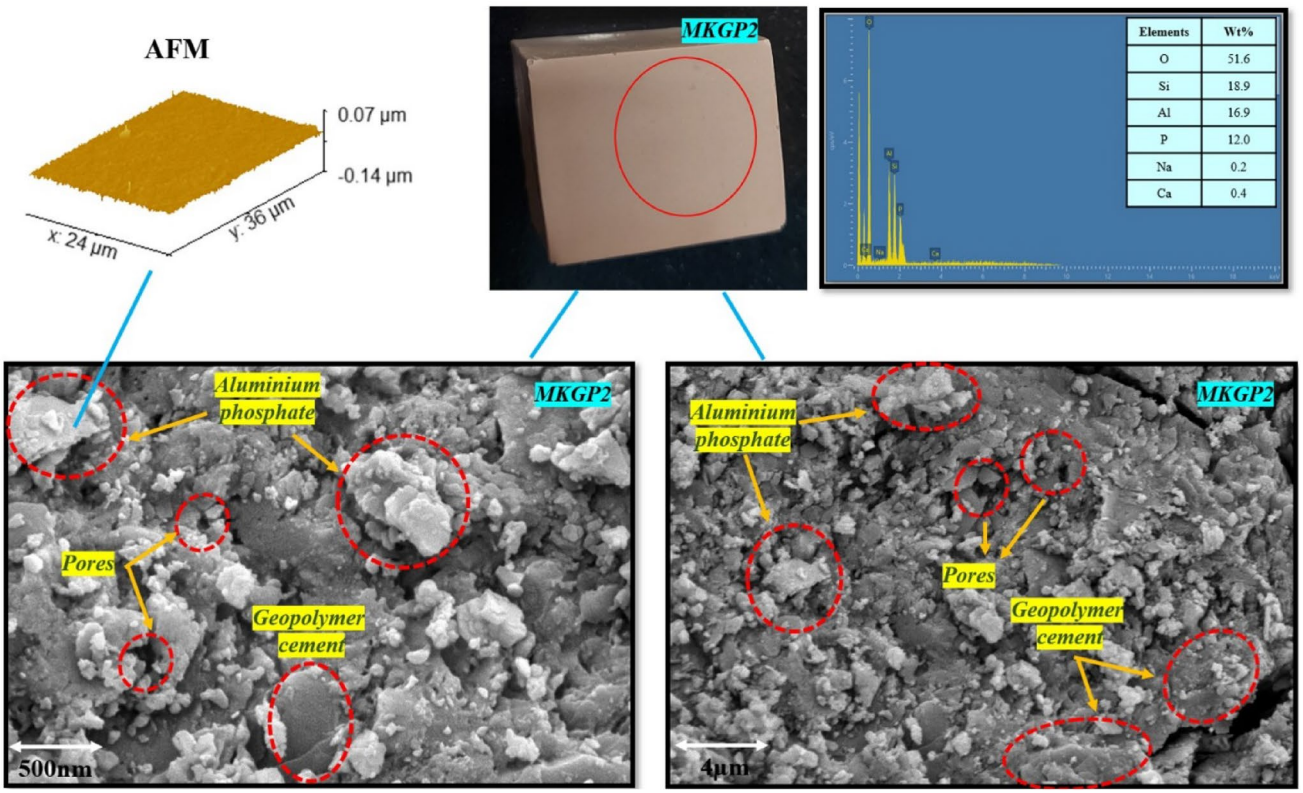

Fig. 14 SEM and AFM micrographs of MKGP2

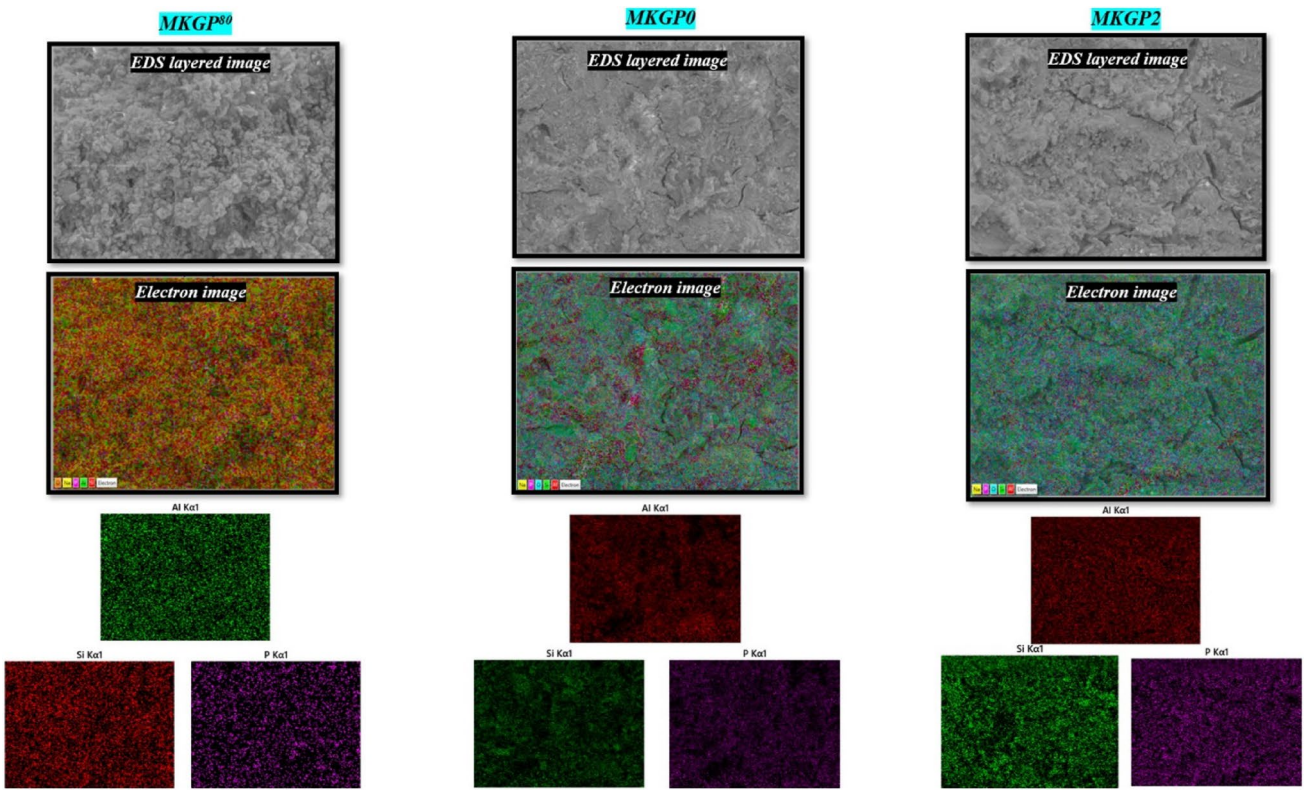

Fig. 15 Elemental mapping of $MKGP^{80}$, MKGP0 and MKGP2

Table 1 SEM Elemental analysis of phosphate geopolymer

Ratio	Sample Id			
	MK	$MKGP^{80}$	MKGP0	MKGP2
Si/Al	1.02	1.01	1.1	1.1
Al/P	–	8.7	1.3	1.5
Si/P	–	8.5	1.1	1.4

pores. MKGP0 shows a gel-printed with a more fractured surface. An almost smooth and uniform image in the surface-modified PEG interlaced composite surface is particularly noteworthy and could be considered as a pointer to better homogeneity as PEG is known to be a self-curing agent (Table 1 and Figs. 12, 13, 14, 15).

8 Conclusion

This study provides a new way to develop a low-cost, high-quality, environmentally friendly metakaolin-based phospo geopolymer and achieves a crack-free surface by the addition of a small amount of PEG 400. The microstructural analysis of control without the addition of PEG matured at ambient temperature and heating to 80 °C compared with PEG-assisted curing. The main crystalline phases of geopolymer cement with and without the addition of PEG are only Berlinite, phosphate of aluminum, and unreacted quartz. Under the optimum dose of PEG at 2%, the surface of geopolymer cement is smooth with the compressive strength of M40 under standard curing age of 28 days. PEG composite formed more amorphous alumino silico phosphates with fewer micropores, a more uniform distribution of gels on the MK lamellae. The water-holding PEG increases the physically/chemically bonded water molecules in the geopolymer network structure thereby improving the thermal resistivity. Thus poly (phospo siloxo) network with Si–O–Al–O–P bond structure obtained at room temperature hardened acid-based geopolymer. The partial replacement of the SiO_4 tetrahedral unit by PO_4 is evident from IR spectral data and thermogram. SEM and AFM microscopic analysis confirmed the surface homogeneity and smoothness in the microstructure. Finally, the surface adsorption of PEG, a phase change material avoided the thermocracking and enhanced the hydrated aluminium phosphate in the SAP network.

Acknowledgements The authors greatly acknowledge the utilization of facilities provided by DST-FIST, Department of Chemistry and SEM facility by NRC, SRM Institute of Science and Technology, Kattankulathur, India. Authors thank the authorities of SRMIST for funding to the research scholars.

Author Contributions NV: Investigation, Methodology, Data curation, and original draft preparation. RJ: Conceptualization, Editing and Supervision, Funding acquisition.

Funding This work was supported by the Department of Science and Technology, the Government of India (GOI), under the grant DST/TDT/WMT/2017 14/03/18, GOI., Kuttuva silicates, Madurai.

Declarations

Competing Interests All the authors declare that there is no conflict of interest.

References

1. J. Davidovits, *Institut Geopolymer, 3rd printing* (Institut Géopolymère, Saint-Quentin, 2008)
2. L. Provis, J.S. John, J. Van Deventer, *Geopolymers: structures, processing, properties and industrial applications* (CRC Press, Boca Raton, 2009)
3. J. Davidovits, Geopolymer Cem **21**, 1–11 (2013)
4. P. Duxson, A. Fernández-Jiménez, J.L. Provis, G.C. Lukey, A. Palomo, J.S.J. van Deventer, J. Mater. Sci. **42**(9), 2917–2933 (2006). https://doi.org/10.1007/s10853-006-0637-z
5. N.B. Singh, S.K. Saxena, M. Kumar, S. Rai, Mater. Today Proc. **15**, 364–370 (2019). https://doi.org/10.1016/j.matpr.2019.04.095
6. Y.S. Wang, Y. Alrefaei, J.G. Dai, Front. Mater. (2019). https://doi.org/10.3389/fmats.2019.00106
7. A. Palomo, M.T. Blanco Varela, M.L. Granizo, F. Puertas, T. Vázquez, M.W. Grutzeck, Cement Concr. Res. **29**, 997–1004 (1999). https://doi.org/10.1016/S0008-8846(99)00074-5
8. D.S. Perera, J.V. Hanna, J. Davis, M.G. Blackford, B.A. Latella, Y. Sasaki, E.R. Vance, J. Mater. Sci. **43**(19), 6562–6566 (2008). https://doi.org/10.1007/s10853-008-2913-6
9. M. Alhawat, A. Ashour, G. Yildirim, A. Aldemir, M. Sahmaran, J. Build. Eng. **50**, 104104 (2022). https://doi.org/10.1016/j.jobe.2022.104104
10. Y.H.M. Amran, R. Alyousef, H. Alabduljabbar, M. El-Zeadani, J. Clean. Prod. (2019). https://doi.org/10.1016/j.jclepro.2019.119679
11. V. Bednarik, J. Melar, M. Vondruska, R. Slavik, J. Inorg. Organomet. Polym. Mater. **21**(1), 9–14 (2010). https://doi.org/10.1007/s10904-010-9424-z
12. M. Zribi, S. Baklouti, Polym. Bull. (2021). https://doi.org/10.1007/s00289-021-03829-0
13. A. Gharzouni, E. Joussein, B. Samet, S. Baklouti, S. Rossignol, J. Non-cryst. Solids **410**, 127–134 (2015). https://doi.org/10.1016/j.jnoncrysol.2014.12
14. A. Gharzouni, L. Vidal, N. Essaidi, E. Joussein, S. Rossignol, Mater. Design **94**, 221–229 (2016). https://doi.org/10.1016/j.matdes.2016.01.043
15. L. Liu, X. Cui, Y. He, S. Liu, S. Gong, Mater. Lett. **66**(1), 10–12 (2012). https://doi.org/10.1016/j.matlet.2011.08.043
16. J. Davidovits, J. Therm. Anal. **35**(2), 429–441 (1989). https://doi.org/10.1007/bf01904446
17. Y.S. Wang, J.L. Provis, J.G. Dai, Cem. Concr. Compos. **93**, 186–195 (2018). https://doi.org/10.1016/j.cemconcomp.2018.07
18. Y.S. Wang, J.G. Dai, Z. Ding, W.T. Xu, Mater. Lett. **190**, 209–212 (2017). https://doi.org/10.1016/j.matlet.2017.01.022
19. M. Mouna Sellami, M. Barre, M. Toumi, J. Inorg. Organomet. Polym. Mater. **30**, 3126–3131 (2020)

20. A.S. Wagh, Advances in Ceramic Matrix Composites X: Proceedings of the 106th Annual Meeting of the American Ceramic Society (Indianapolis, IN). Vol. 107. (2004)
21. M. Zribi, B. Samet, S. Baklouti, J. Solid State Chem. **281**, 121025 (2020). https://doi.org/10.1016/j.jssc.2019.121025
22. M. habbouchi, K. Hosni, M. Mezni, C. Zanelli, M. Doggy, M. Dondi, E. Srasra, Appl. Clay Sci. **146**, 510–516 (2017). https://doi.org/10.1016/j.clay.2017.07.00
23. M. Zribi, B. Samet, S. Baklouti, J. Non-Cryst. Solids **511**, 62–67 (2019). https://doi.org/10.1016/j.jnoncrysol.2019.01
24. L. Gao, Y. Zheng, Y. Tang, J. Yu, X. Yu, B. Liu, Heliyon **6**(4), e03853 (2020). https://doi.org/10.1016/j.heliyon.2020.e03853
25. T. Dong, S. Xie, J. Wang, Z. Chen, Q. Liu, Q J. Aust. Ceram. Soc. (2019). https://doi.org/10.1007/s41779-019-00376-w
26. H.I. Riyap, F. Kenne Tazune, D. Fotio, H.K. Tchakoute, C.P. NanseuNjiki, C.H. Ruscher, J. Inorg. Organomet. Polym. Mater. **31**, 3301–3323 (2021). https://doi.org/10.1007/s10904-021-01949-8
27. H.K. Tchakouté, C.H. Rüscher, E. Kamseu, F. Andreola, C. Leonelli, Appl. Clay Sci. **147**, 184–194 (2017). https://doi.org/10.1016/j.clay.2017.07.036
28. H.I. Riyap, B.K. Ngongang, H.K. Tchakouté et al., Silicon **14**, 10535–10558 (2022). https://doi.org/10.1007/s12633-022-01786-5
29. R. Gupta, P. Bhardwaj, D. Mishra, M. Prasad, S.S. Amritphale, J. Inorg. Organomet. Polym. Mater. **27**(2), 385–398 (2016). https://doi.org/10.1007/s10904-016-0461-0
30. O.M. Jensen, P.F. Hansen, Cem. Concr. Res. **32**(6), 973–978 (2002). https://doi.org/10.1016/s0008-8846(02)00737-8
31. V. Mechtcherine, H.W. Reinhardt, *Application of Super Absorbent Polymers (SAP) in Concrete Construction* (Springer, Cham, 2012)
32. O. Mikhailova, P. Rovnaník, Proc. Eng. **151**, 222–228 (2016). https://doi.org/10.1016/j.proeng.2016.07.379
33. V. Mathivet, J. Jouin, A. Gharzouni, I. Sobrados, H. Celerier, S. Rossignol, M. Parlier, J. Non-cryst. Solids **512**, 90–97 (2019). https://doi.org/10.1016/j.jnoncrysol.2019.02.025
34. H. Lin, H. Liu, Y. Li, X. Kong, Cem. Concr. Res. **144**, 106425 (2021). https://doi.org/10.1016/j.cemconres.2021.106425
35. C. Nobouassia Bewa, H.K. Tchakouté, D. Fotio, C.H. Rüscher, E. Kamseu, C. Leonelli, J. Asian. Ceam. Soc. (2018). https://doi.org/10.1080/21870764.2018.1507660
36. J. Jouin, H. Celerier, L. Ouamara, N. Tessier-Doyen, S. Rossignol, J. Am. Ceram. Soc. **104**(10), 5445–5456 (2021). https://doi.org/10.1111/jace.17929
37. A. Katsiki, T. Hertel, T. Tysmans, Y. Pontikes, H. Rahier, Materials **12**(3), 442 (2019). https://doi.org/10.3390/ma12030442
38. X. Zhang, J. Qiao, W. Zhang, F. Cheng, Z. Yin, Z. Huang, X. Min, J. Mater. Sci. **53**(18), 13067–13080 (2018). https://doi.org/10.1007/s10853-018-2531-x
39. X. Cui, L. Liu, Y. He, J. Chen, J. Zhou, Mater. Chem. Phys. **130**(1–2), 1–4 (2011). https://doi.org/10.1016/j.matchemphys.2011.06.039
40. H. Celerier, J. Jouin, N. Tessier-Doyen, S. Rossignol, J. Non-cryst. Solids (2018). https://doi.org/10.1016/j.jnoncrysol.2018.09.005
41. N. Vanitha, R. Jeyalakshmi, Inorg. Chem. Commun. **153**, 110758 (2023). https://doi.org/10.1016/j.inoche.2023.110758
42. N. Vanitha, T. Revathi, M. Sivasakthi, R. Jeyalakshmi, J. Solid State Chem. **312**, 123188 (2022). https://doi.org/10.1016/j.jssc.2022.123188
43. H.K. Tchakouté, C.H. Rüscher, S. Kong, E. Kamseu, C. Leonelli, J. Solgel Sci. Technol. **78**(3), 492–506 (2016). https://doi.org/10.1007/s10971-016-3983-6
44. R.A. Khan, C. Gupta, Int. J. Res. Advent Technol. (IJRAT) **11**, 1–7 (2020)